Wetting phenomena for mercury on sapphire

2001 J. Phys.: Condens. Matter 13 R297

(http://iopscience.iop.org/0953-8984/13/15/202)

INSTITUTE OF PHYSICS PUBLISHING JOURNAL OF PHYSICS: CONDENSED MATTER

J. Phys.: Condens. Matter **13** (2001) R297–R319 www.iop.org/Journals/cm PII: S0953-8984(01)07649-4

TOPICAL REVIEW

Wetting phenomena for mercury on sapphire

M Yao and Y Ohmasa

Department of Physics, Graduate School of Science, Kyoto University, Kyoto 606-8502, Japan[1]

Received 1 March 2001

Abstract

In the present article we make a brief review of our recent studies on the wetting behaviour of mercury on a sapphire substrate. The prewetting phase diagram, and the temperature and pressure dependence of the prewetting order parameter and its fluctuation are presented. The interplay between the wetting transition and the metal–non-metal transition, and the crossover from wetting to critical adsorption are discussed. The experimental techniques that have been newly developed to study the mercury wetting film under high temperature and high pressure are also explained.

Contents

1. Introduction

Wetting is a kind of three-phase-coexistence phenomenon [1]. The contact angle Θ defined in figure 1 gives the degree of wetting and is described by the Young equation:

$$\cos\Theta = \frac{\sigma_{SV} - \sigma_{SL}}{\sigma_{LV}} \tag{1}$$

where the σ are the interfacial tensions and the subscripts L, V and S denote the liquid, vapour and substrate, respectively. In 1977 Cahn [2] studied the asymptotic behaviour of the Young equation on approaching the liquid–gas critical point, and predicted the necessity of wetting near the critical point (i.e. the critical point wetting): there must be a temperature T_w below the critical temperature T_c that makes the contact angle vanish. This type of wetting phenomenon occurs either as a first-order or a second-order phase transition, and in the former case the

[1] Telephone: +81-75-753-3774; fax: +81-75-753-3780.

prewetting line, on which the wetting film changes abruptly from thin to thick, starts at T_w and terminates at the prewetting critical point (CPW). It is believed from thermodynamic considerations that the prewetting line merges tangentially into the saturated vapour pressure (SVP) curve of the bulk liquid [3]. The prewetting transition may be treated as a liquid–gas phase transition in two dimensions (2D), and Monte Carlo simulations [4] suggested that the critical phenomena in the vicinity of the CPW belong to the 2D Ising universality class, though there have still been few experimental studies on the criticality [5, 6]. Ebner and Saam [7] also predicted the wetting transition in 1977, using a density functional method. The same authors [8] showed later that the critical point wetting does not necessarily occur in the presence of long-range forces. Thus experimental work has been desirable for a long time.

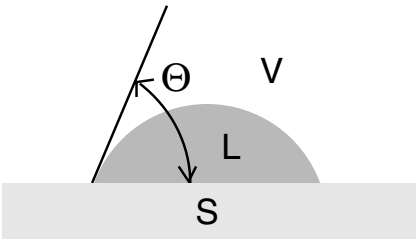

Figure 1. A small droplet (L) sitting at the interface between a solid substrate (S) and a bulk vapour phase (V). Θ is the contact angle.

The first clear experimental evidence for the prewetting transition was presented by Rutledge and Taborek [9], who observed a helium wetting film on a caesium substrate by a micro-balance technique. Liquid helium is famous for its 'high wettability' (high degree of ability to wet) when placed on various materials. However, it does not wet Cs exceptionally well at very low temperatures owing to the repulsion between the He atom and the outermost electrons of Cs [10]. Subsequently, prewetting transitions were found in several fluid systems, either near the liquid–gas critical point [11–14] or near the liquid–liquid critical point [5,6,15]. Mercury on a sapphire substrate [12, 16] is the first liquid-metal system found to undergo the prewetting transition. Liquid Hg wets most metallic substances when their surfaces are free from oxides or sulphides, and it often reacts with the metallic surfaces to form amalgams. In contrast, liquid mercury hardly wets non-metallic substances such as glasses or sapphire at all under ambient conditions.

The 'wettability' (ability to wet) in the van der Waals systems can be generally treated by the Dzyaloshinskii, Lifshitz and Pitaevskii (DLP) theory [17], in which the retarded and non-additivity effects of the inter-atomic interactions are rigorously taken into account although short-range effects such as solvation are not properly included. The theory is often used in a simplified version such as the Israelachvili approximation [18] to calculate the Hamaker constant for macroscopic systems. The most important quantities in the DLP theory are the dielectric permeability and the imaginary frequency-dependent dielectric functions.

The effective potential between the constituent ions in liquid metals consists of two terms [19]: the first one is the direct bare Coulomb repulsion between the ions; and the second one is the indirect, more attractive, part arising from the electron–ion interactions. In the latter the screening of ions with electrons plays a key role. Since the second term includes the dielectric function that depends strongly on the density of the conduction electrons, the effective inter-atomic potential in liquid metals varies with density in contrast to the case for insulating liquids. When the density of the liquid metal is further reduced by raising the temperature beyond the critical point, the metallic nature is eventually changed into a non-

metallic one [20]. In the metal–non-metal (M–NM) transition range, an energy gap between the valence and conduction bands opens up, giving rise to a dramatic change in the dielectric properties (i.e. the polarization catastrophe [21]). Thus it may be interesting to discuss the interplay between the wetting transition and the M–NM transition.

It is well known that the density–density correlation length ξ_{3D} and hence many quantities such as the compressibility χ_{3D} become divergently large on approaching the bulk liquid–gas critical point. Like the three-dimensional (3D) critical phenomena, large interfacial fluctuations are expected to appear near the CPW, where the 2D compressibility, defined as

$$\chi_{2D} = (\partial\Gamma/\partial\mu)_T$$

should become divergently large. Here Γ is the coverage and μ is the chemical potential. From the experimental point of view, the 3D critical fluctuations are usually probed by means of small-angle scattering measurements in which visible light, x-rays or neutrons are utilized. Unfortunately no such well-established technique has been applied to study the prewetting critical phenomena. Recently we have found that thermal radiation can be utilized to detect 2D critical fluctuations [22].

Critical adsorption is an interfacial phenomenon that is controlled by the 3D critical fluctuations [23]. On the basis of a scaling argument, the density profile is described by using the bulk critical exponents. Since the CPW is often located near the bulk critical point, there may be a possibility that the 3D critical fluctuations could influence the wetting phenomena which have 2D character. A crossover from complete wetting to critical adsorption was theoretically studied by Dietrich [24], but there has been no experimental work so far concerning this intriguing problem.

In the present article we make a brief review of our recent studies on the wetting behaviour of mercury on a sapphire substrate. The rest of this article is divided into the following sections. In section 2 we will give relevant information on the physical properties of bulk fluid mercury with emphasis on the M–NM transition. In section 3 the first evidence for the prewetting transition of mercury and the prewetting phase diagram will be described. More rigorous experimental proof of the prewetting transition will be given in section 4, where a newly developed ellipsometric technique that can be applied to high-temperature and high-pressure conditions will also be explained. On the basis of these ellipsometric measurements, the properties of the mercury wetting film will be discussed in section 5. In section 6 we will discuss how the density profile of the wetting film changes as the temperature increases toward the bulk critical temperature in connection with the critical adsorption. In section 7 we will show that the thermal radiation can be utilized to probe the interfacial fluctuations, and we will present direct evidence for the 2D critical fluctuations. In the last section we will give a brief summary.

2. Physical properties of bulk fluid mercury

Since the liquid–gas critical point of mercury is located at relatively low temperature (1478 °C) and pressure (167 MPa), various physical properties have been investigated over a wide density range including the supercritical conditions [20]. Experimental studies on the electronic properties have revealed that a metal–non-metal (M–NM) transition occurs at densities near 9 g cm^{-3}, which is appreciably larger than the critical density (5.8 g cm^{-3}). The strongest evidence for the M–NM transition may be the vanishing of the Knight shift [25] on approaching the M–NM transition from the metallic side, and the vanishing of the optical gap [26] from the non-metallic side (see figure 2). Figure 3 shows the phase diagram on the pressure and temperature (P, T) plane, where the M–NM transition range is denoted by the hatching.

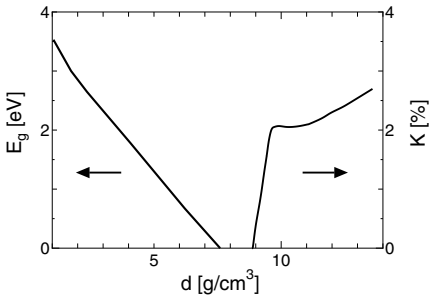

Figure 2. The density dependence of the optical gap E_g [26] and the Knight shift K [25] for bulk fluid mercury.

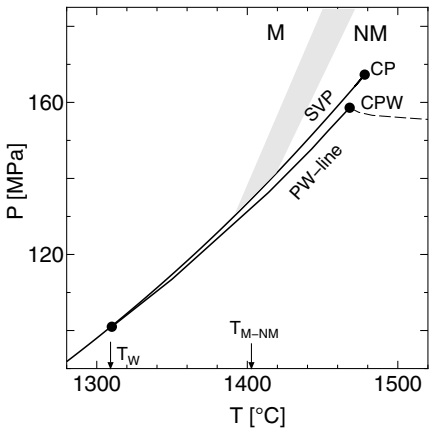

Figure 3. The (P, T) phase diagram of fluid mercury and the mercury–sapphire system. The solid lines 'SVP' and 'PW-line' indicate the saturated vapour pressure and prewetting lines, respectively. T_w and T_{M-NM} indicate the wetting temperature and the metal–non-metal (M–NM) transition temperature, respectively. The M–NM transition range is denoted by the hatching. The solid circles 'CP' and 'CPW' are the bulk liquid–gas critical point and the prewetting critical point. The dashed line which starts from the CPW is the locus of the maximum of the 2D compressibility χ_{2D}.

Theoretical *ab initio* computer simulations, which were originally developed by Car and Parrinello [27], were applied to expanded liquid Hg by Kresse and Hafner [28], who calculated the radial distribution functions and the density of states. As expected from the experimental data shown in figure 2, it has been concluded that the M–NM transition in liquid Hg is mainly due to the vanishing of the overlap between the 6s and 6p bands.

An issue of considerable interest is that the M–NM transitions in the liquid state are, in most cases, not purely electronic transitions but are accompanied by changes in the thermodynamic properties such as the equation of state [29] and the sound velocity [30]. Recent x-ray diffraction measurements [31] reveal that the nearest-neighbour distance is elongated from 3.0 Å to about 3.3 Å when the density decreases from 9 to 6 g cm^{-3}, which is different from the expected lattice-gas-like behaviour of expanded liquid: when the liquid is expanded, the coordination number decreases almost linearly with density, keeping the nearest-neighbour distance nearly constant [32–35]. Furthermore, a slow dynamics with a relaxation time of about two nanoseconds has been found in the M–NM transition range from sound attenuation measurements [36].

3. Discovery of the prewetting transition of Hg on sapphire

The prewetting transition of mercury on a sapphire substrate was discovered during measurements of the optical reflectivity of the interface between sapphire and Hg vapour [12, 39]. The reflectivity was measured for incident light nearly normal to the interface by using a long optical reflectivity cell (figure 4). The cell consists of a molybdenum cylinder with an inner diameter of 5 mm, which is closed at one end by an 80 mm long synthetic sapphire window. The sapphire window has a cylindrical shape with optically polished flat ends, one of which is in contact with the mercury sample in the hot part. The long cell is necessary for optimal elimination of temperature gradients. The cell was mounted in a specially constructed autoclave with a high-pressure window and an internal electric resistance furnace which is thermally isolated from the vessel walls. The cell is connected to a reservoir maintained at the same pressure as the autoclave, which is pressurized by argon gas.

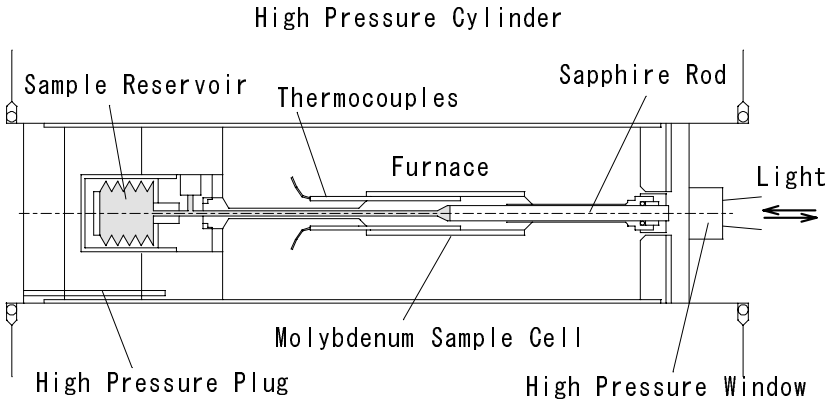

Figure 4. The cell assembly used for the optical reflectivity measurements [39].

In figure 5, the reflectivity of fluid Hg behind the sapphire optical window is shown for the photon energy of 1.27 eV as a function of pressure at 1300 °C, 1450 °C and 1474 °C [12]. At 1300 °C the observed reflectivity decreases with increasing pressure and abruptly jumps to a large value at the vapour–liquid transition. In the vapour phase the reflectivity R_n normal to the interface between the sapphire and the Hg vapour is well reproduced by the Fresnel formula [37]:

$$R_n = |r_{SV}|^2 \tag{2}$$

where r_{SV} is the complex Fresnel index given by

$$r_{SV} = \frac{\tilde{n}_S - \tilde{n}_V}{\tilde{n}_S + \tilde{n}_V}. \tag{3}$$

Here $\tilde{n}_V = n_V + ik_V$ and $\tilde{n}_S = n_0 = 1.77$ are the complex refractive indexes of Hg vapour and sapphire, respectively. When $k_V = 0$, n_V is calculated from the Lorentz–Lorenz relation

$$n_V = \sqrt{\frac{1 + 2\alpha d}{1 - \alpha d}} \tag{4}$$

where α is a number proportional to the polarizability of an isolated atom and d is the density of the vapour.

At 1450 °C, on the other hand, the observed reflectivity shows a downward deviation from the Fresnel formula above 140 MPa and begins to increase around 150 MPa, which is

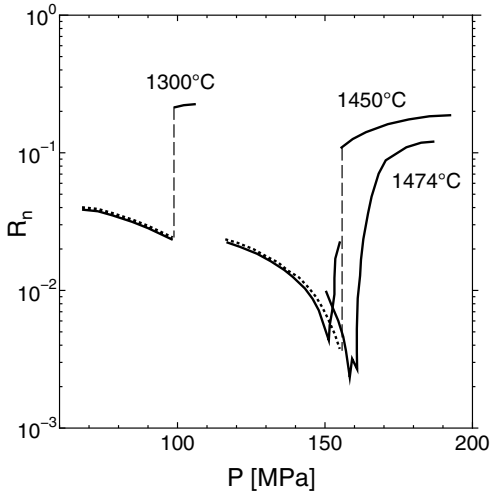

Figure 5. Reflectivity at normal incidence, R_n, for fluid Hg behind the sapphire optical window at 1.27 eV at 1300 °C, 1450 °C and 1474 °C [12]. The dotted lines show the reflectivity calculated for the mercury bulk vapour phase from the Fresnel formula (2) and the Lorentz–Lorenz relation (4).

appreciably lower than the vapour–liquid transition pressure. We interpreted the anomalous behaviour by assuming that a wetting film is formed on the sapphire substrate [12]. The deviation from the Fresnel formula should stem from destructive or constructive interference between the reflected lights from the sapphire/Hg-film interface and from the Hg-film/vapour interface. Then, instead of the Fresnel equation, the reflectivity can be written as [38]

$$R_n = \left| \frac{r_{SL} + r_{LV} \exp(2i\Delta)}{1 + r_{SL} r_{LV} \exp(2i\Delta)} \right|^2 \tag{5}$$

with

$$\Delta = \frac{2\pi l_{slab} \tilde{n}_L}{\lambda} \tag{6}$$

where l_{slab} is the thickness of the wetting film and λ is the wavelength of the light. Here we assume that the intruding film has a slab shape, whose density profile is illustrated in figure 6(a). We assume further that the film has the same density and the same optical properties as the coexisting bulk liquid at the corresponding saturated pressure P_{sat} at each temperature. As shown in figure 7(a), l_{slab} jumps at the prewetting transition and the amount of the jump decreases with increasing pressure, vanishing at the prewetting critical pressure [12]. In figure 3 the prewetting line is shown on the (P, T) plane together with the bulk saturated vapour pressure (SVP) curve [12, 39]. The prewetting line starts from T_w, around 1310 °C, and terminates at the CPW located at 1468 °C and 158.6 MPa. It should be noted that the CPW exists at a lower temperature than the critical point of bulk fluid. The same trend has been observed in other one-component fluids such as He on Cs [9] and Rb [14] as well as binary liquid mixtures such as methanol–cyclohexane [5]. In the case of Hg on Mo or Nb [13] and K–KCl [15], on the other hand, the CPW lies at higher temperature than the bulk critical point.

Anomalous behaviour of the reflectivity was also observed in the prewetting supercritical region. The pressure dependence of R_n at 1474 °C is shown in figure 5 as an example [12]. At supercritical temperatures no discontinuous jump was observed in the variation of the film

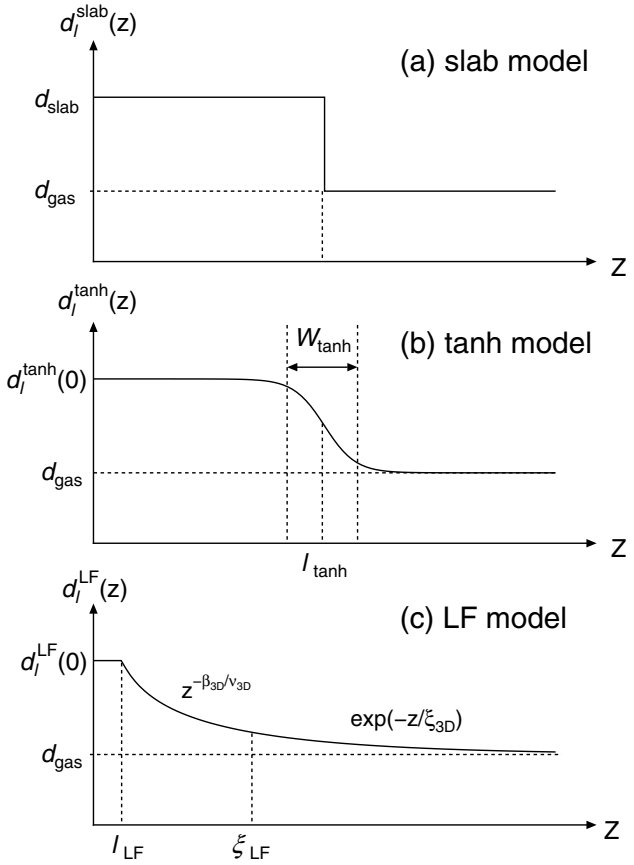

Figure 6. Density profile models for the wetting film used in the present work. (a) indicates the slab model, (b) the slowly varying tanh profile (see equation (11)) and (c) the power-law–exponential-type profile (see equation (14)).

thickness l_{slab} with pressure, but the rate of increase of l_{slab} becomes very large in a narrow pressure range (see figure 7(b)). Since this behaviour resembles the rapid increase of density with pressure in the 3D supercritical region, the steepest increase of l_{slab} may be assigned to the maximum of the 2D compressibility χ_{2D}. A similar observation was made for the He/Cs interface [9]. In figure 3 the dashed line which starts from the CPW is the locus of the maximum χ_{2D} on the (P, T) plane. The prewetting line and the locus of the maximum χ_{2D} are replotted on the plane of reduced pressure P/P_{sat} and temperature T in figure 8 [12, 39]. The maximum χ_{2D} appears at considerably lower pressures than the simple extrapolation of the prewetting line.

4. Confirmation of the prewetting transition

In the preceding section anomalous reflectivity has been interpreted by assuming a prewetting transition at the Hg/sapphire interface. That is, the prewetting transition is a sufficient condition for the anomalous reflectivity but not a necessary condition. Therefore we must confirm the prewetting transition in another more rigorous way.

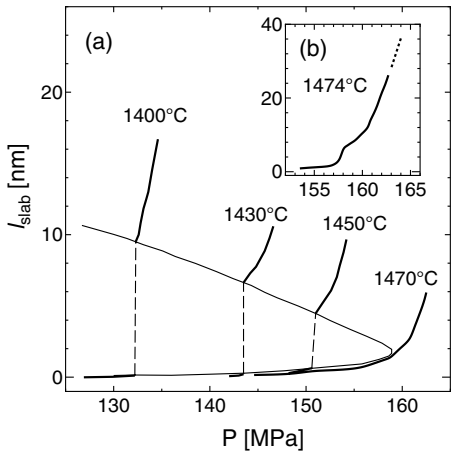

Figure 7. The thickness of the wetting film l_{slab} in the (a) prewetting subcritical and (b) prewetting supercritical region [12]. l_{slab} is estimated from a slab model under the assumption that the density of the wetting film d_{slab} and the optical properties are the same as those of the coexisting bulk liquid at the corresponding saturated pressure P_{sat} at each temperature.

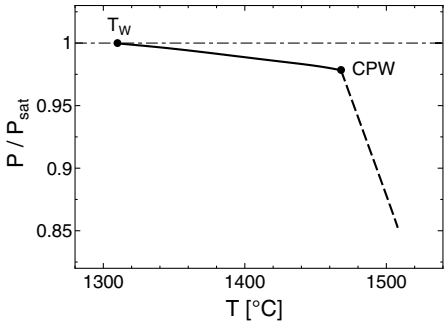

Figure 8. The prewetting line (solid line) and the locus of the maximum χ_{2D} (dashed line) plotted on the plane of reduced pressure P/P_{sat} and temperature T [12,39]. The dash–dotted line indicates the saturated vapour curve ($P/P_{sat} = 1$).

Ellipsometry is a method widely used to investigate interfacial properties [40]. In conventional ellipsometry, the complex reflectivity ratio (i.e. ellipticity):

$$\rho = r_p/r_s = \tan\psi \exp(i\delta)$$

of p- and s-polarized light is measured. However, from the viewpoint of experimental technique, this method is not suitable for experiments under high temperature and high pressure. The most serious problem is that of how to determine the phase shift δ, because δ is strongly affected by the birefringence of the sapphire window and the birefringence is highly temperature dependent [41]. Thus, instead of ψ and δ, we have measured the reflectance intensity for p- and s-polarized lights, $R_p = |r_p|^2$ and $R_s = |r_s|^2$, separately [42–44].

For this purpose we adopt a wedge-shape sapphire rod as the optical window of the cell [42–44] (see figure 9). The wedge is formed by two flat surfaces with an opening angle of 90°, so the incident light is reflected twice and goes back in the initial direction. The incident angle in each reflection is 45°. Owing to the birefringence, the sapphire window works as a polarizing prism by itself, and consequently it splits the depolarized incident light into p- and

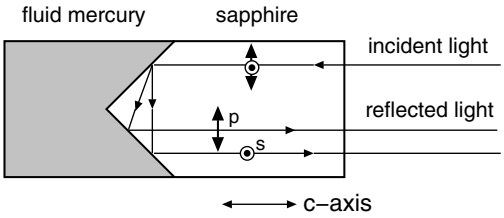

Figure 9. A schematic illustration of the optical paths through the sapphire rods for the 45°-reflection ellipsometric measurements [42–44].

s-polarized reflected lights. Our experimental set-up for the ellipsometric measurements is schematically illustrated in figure 10 [44]. A further advantageous feature of the 45° reflection is that it is very sensitive to the formation of wetting film. This is because

$$R_{\mathrm{s}} = \left| \frac{n_0 - \sqrt{2\tilde{n}^2 - n_0^2}}{n_0 + \sqrt{2\tilde{n}^2 - n_0^2}} \right|^2 \tag{7}$$

$$R_{\mathrm{p}} = \left| \frac{\tilde{n}^2 - n_0\sqrt{2\tilde{n}^2 - n_0^2}}{\tilde{n}^2 + n_0\sqrt{2\tilde{n}^2 - n_0^2}} \right|^2 \tag{8}$$

and hence

$$R_{\mathrm{p}} = R_{\mathrm{s}}^2 \tag{9}$$

always holds for the 45° reflection whenever the optical window (e.g. sapphire) is in direct contact with bulk phase (e.g. vapour or liquid mercury) [42–44]. In the presence of the wetting

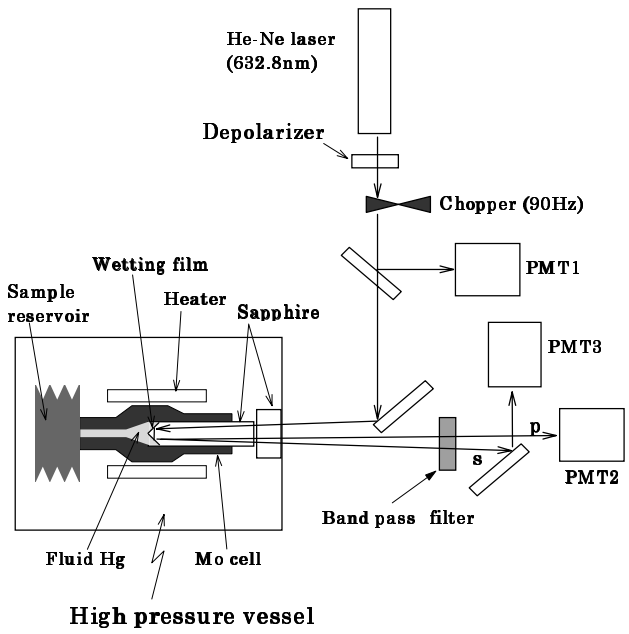

Figure 10. The experimental set-up for the 45°-reflection ellipsometric measurements [44].

film, however, this equation does not hold any longer owing to the interference effects. In fact figure 11 demonstrates how R_p and R_s^2 change with the thickness l_{slab} of the Hg film when, for example, the density of the wetting film and the Hg vapour are 7.0 g cm^{-3} and 3.0 g cm^{-3}, respectively. As l_{slab} increases, R_s^2 decreases first and then increases above 5 nm, while R_p increases monotonically. Therefore, by comparing R_p and R_s^2, we can detect the formation of the wetting film with high precision.

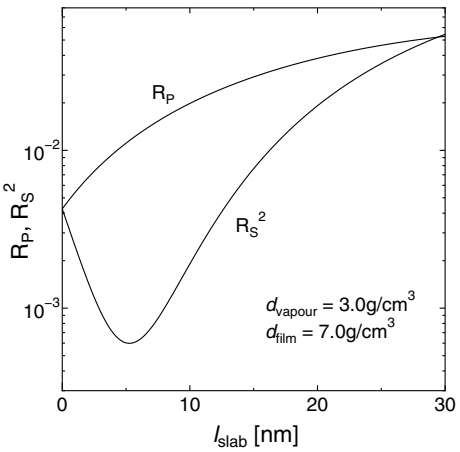

Figure 11. The reflectances calculated as functions of film thickness l_{slab} for the s-polarized light (R_s) and for the p-polarized light (R_p) in the 45°-reflection geometry [44]. They were calculated for a typical case where the density of the mercury wetting film is 7.0 g cm^{-3} and the density of the coexisting vapour is 3.0 g cm^{-3}.

In figure 12 representative results for R_p and R_s^2 for the Hg/sapphire interface are shown at the wavelength λ of 632.8 nm as a function of pressure at 1328 °C and 1440 °C [44]. The equation $R_s^2 = R_p$ holds in the low-pressure vapour phase as well as in the liquid phase, while at the intermediate pressures the relation is violated, indicating the formation of the wetting film [42–44]. The existence of the prewetting transition is unambiguously confirmed from the observed discontinuous changes in both R_p and R_s^2. At 1328 °C, which is not far from T_w, the wetting film is evident only in a narrow pressure range between the prewetting and the liquid–vapour transitions. The plateau at low pressures is due to the total reflection. At 1440 °C, on the other hand, the wetting film is definitely formed even below the prewetting transition pressure.

5. Properties of mercury wetting film

It is interesting to note that the wetting temperature T_w is lower than the temperature T_{M-NM} at which the M–NM transition region meets the SVP curve, as shown in figure 3. This is reminiscent of the relation between the normal-to-superfluid transition line (i.e. the λ-line) of bulk helium and the prewetting line of helium on caesium [45]. In the He film a Kosterlitz–Thouless transition is observed at temperatures and pressures lying along the extension of the λ-line into the vapour phase [45]. By analogy, this may raise the intriguing question of whether a M–NM transition occurs in the Hg film on sapphire.

In section 3 we made a rough estimation of the film thickness by assuming that the intruding film has the same density as the coexisting bulk liquid at the saturated pressure P_{sat}. However, this is not always true, because the density profile of the wetting film is determined in such

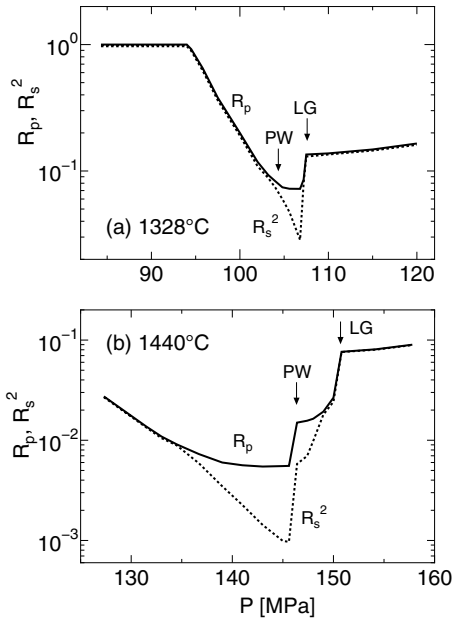

Figure 12. Representative results for R_p (solid lines) and R_s^2 (dotted lines) in the 45°-reflection geometry at the wavelength λ of 632.8 nm, as functions of pressure at 1328 °C and 1440 °C [44]. 'PW' and 'LG' indicate the prewetting point and liquid–gas transition point, respectively.

a way that the total grand potential is minimized under the influence of the surface field. In the case of liquid metals the theoretical treatment should be more complicated because the inter-atomic interactions are density dependent, as mentioned in the introduction.

In this section we study the properties of the wetting film. For this purpose, we deduce the effective density of the wetting film within the framework of the slab model (see figure 6(a)). We assume that the density dependence of the complex refractive index for the wetting film is the same as that for bulk Hg. Figure 13 illustrates the density dependence of the complex refractive index $n + ik$ for the bulk Hg [44]. It should be noted that both n and k for Hg behave

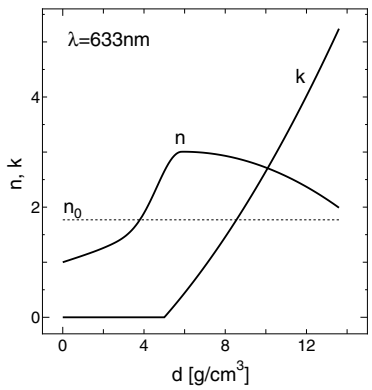

Figure 13. The density dependence of the complex refractive index $n + ik$ for the bulk fluid mercury [44]. The dashed line indicates the refractive index n_0 of the sapphire substrate.

very differently from those for normal insulating fluids, for which $n - 1$ is nearly proportional to the density and $k = 0$. This specific feature of Hg is an advantage in determining d_{slab} and l_{slab} for the wetting film. The coverage Γ_{slab} is simply the product of $d_{slab} - d_{gas}$ and l_{slab} in the slab model.

Representative results for d_{slab}, l_{slab} and Γ_{slab} at 1386 °C are shown in figure 14 [44]. At the prewetting transition both d_{slab} and l_{slab} change discontinuously. Compared with the previous results for l_{slab} at e.g. 1400 °C shown in figure 7, the present l_{slab} is much larger on the thin-film side but comparable on the thick-film side. The discrepancy may stem from the procedure in the previous analysis where the density of the wetting film is fixed to that of the coexisting liquid. With further increasing pressure, l_{slab} and consequently Γ_{slab} increase sharply in accordance with the expectation that the wetting film grows into a macroscopic liquid film. However, d_{slab} tends to be saturated below 7.5 g cm^{-3}, which is considerably smaller than the corresponding bulk density of around 9 g cm^{-3}.

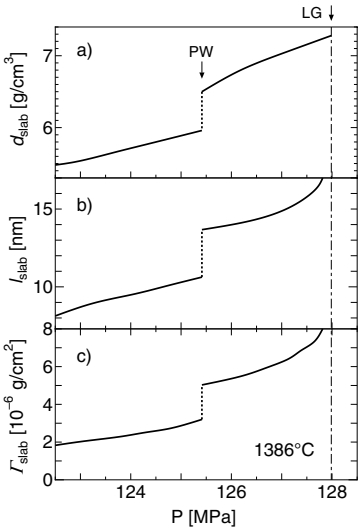

Figure 14. Representative results for the density d_{slab}, the thickness l_{slab} and the coverage Γ_{slab} of the wetting film estimated by using the slab model at 1386 °C [44].

The densities of the coexisting thin and thick films are plotted as a function of temperature in figure 15 together with the bulk coexistence curve [44]. In accordance with a simple argument on the prewetting transition, the density of the thin wetting film is larger than that of bulk vapour and it seems to increase with increasing temperature. However, unexpectedly, the density of the thick wetting film remains about 7 g cm^{-3}, which is much smaller than that of bulk liquid. This implies that the wetting film is somewhat expanded compared with the corresponding bulk liquid. It may be instructive to point out that the wetting film in the K–KCl system is also different from the stable bulk liquid [46]. Since the M–NM transition in bulk Hg occurs at densities of 8 to 9 g cm^{-3} and the transition density is expected to become larger with lowering dimension, it may be concluded on the basis of our observation that the Hg wetting film is non-metallic.

This finding may be supported by the theory of long-range dispersion forces between polarizable media (i.e. DLP theory [17]). When the thickness of the wetting film is small enough and the retardation effect can be neglected, the van der Waals chemical potential is

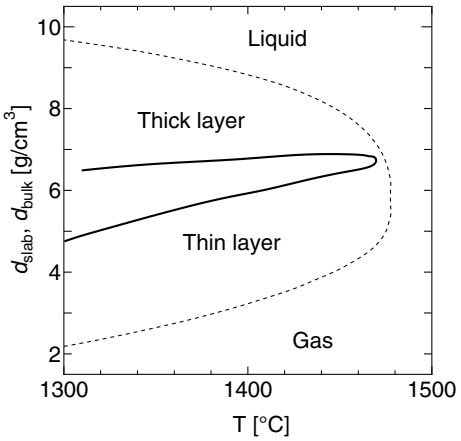

Figure 15. The solid line indicates the density of the wetting film at the prewetting transition. The dashed line indicates the density of the bulk fluid mercury at the liquid–gas coexistence.

simplified as follows:

$$\mu = -\frac{\hbar}{16\pi^2\rho l_{\rm slab}^3}\int_0^\infty {\rm d}\omega \int_0^\infty {\rm d}x\; x^2(f^{-1}{\rm e}^x+1)^{-1} \simeq -\frac{\hbar}{8\pi^2\rho l_{\rm slab}^3}\int_0^\infty {\rm d}\omega\; f \tag{10}$$

where

$$f = \frac{\epsilon_{\rm sub}({\rm i}\omega)-\epsilon_{\rm slab}({\rm i}\omega)}{\epsilon_{\rm sub}({\rm i}\omega)+\epsilon_{\rm slab}({\rm i}\omega)}\,\frac{\epsilon_{\rm slab}({\rm i}\omega)-\epsilon_{\rm gas}({\rm i}\omega)}{\epsilon_{\rm slab}({\rm i}\omega)+\epsilon_{\rm gas}({\rm i}\omega)}$$

and ρ is the number density of mercury atoms in the wetting film. $\epsilon_{\rm sub}({\rm i}\omega)$, $\epsilon_{\rm slab}({\rm i}\omega)$ and $\epsilon_{\rm gas}({\rm i}\omega)$ are dielectric functions for the sapphire substrate, the wetting film and the coexisting mercury gas phase, respectively, at imaginary frequencies iω, and these quantities are calculated from the optical conductivity by using the Kramers–Kronig relation. When the density is higher than 9 g cm^{-3}, fluid mercury has metallic nature and its dielectric function diverges at $\omega = 0$. Hence,

$$\epsilon_{\rm slab}({\rm i}\omega) > \epsilon_{\rm sub}({\rm i}\omega) \qquad \text{and} \qquad \epsilon_{\rm slab}({\rm i}\omega) > \epsilon_{\rm gas}({\rm i}\omega)$$

at low frequencies. Then it follows from the DLP theory that μ is positive, leading to non-wetting [47]. When the density is decreased below 9 g cm^{-3}, on the other hand, the properties of mercury change to non-metallic with a finite energy gap, which implies that the dielectric function has a finite value at $\omega = 0$. Thus $\epsilon_{\rm slab}({\rm i}\omega)$ decreases and becomes smaller than $\epsilon_{\rm sub}({\rm i}\omega)$ over a wide range of the frequency ω:

$$\epsilon_{\rm slab}({\rm i}\omega) < \epsilon_{\rm sub}({\rm i}\omega) \qquad \text{and} \qquad \epsilon_{\rm slab}({\rm i}\omega) > \epsilon_{\rm gas}({\rm i}\omega).$$

Therefore, μ is expected to decrease with decreasing $d_{\rm slab}$ [47]. Our preliminary calculation of μ using the dielectric function at various densities [48] shows that μ changes its sign from positive to negative when the density $d_{\rm slab}$ is decreased below 8 g cm^{-3}. This may be why the sapphire substrate prefers a wetting film with density lower than that of the coexisting bulk liquid.

To close this section, the coverage $\Gamma_{\rm slab}$ of the coexisting thin and thick films is shown as a function of temperature in figure 16. The coexistence curve in the vicinity of the prewetting critical point (dotted line) is drawn in such a way that the critical exponent of the order parameter takes the value for the 2D Ising model (i.e. 1/8), though another possibility cannot be excluded

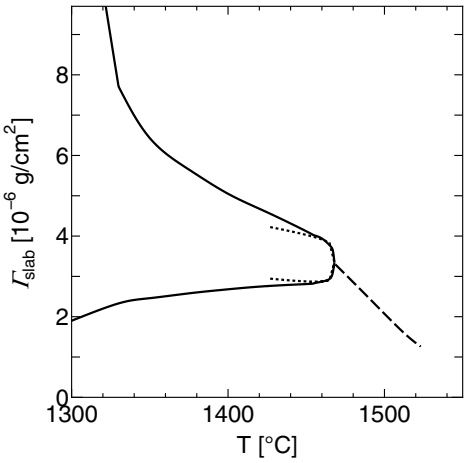

Figure 16. The coverage Γ_{slab} of the coexisting thin and thick films as a function of temperature. The dotted line in the vicinity of the prewetting critical point is drawn in such a way that the critical exponent of the order parameter takes the value for the 2D Ising model (i.e. 1/8). The dashed line in the supercritical phase denotes Γ_{slab} along the locus of the maximum of the 2D compressibility χ_{2D}.

at this stage. The dashed line in the supercritical phase denotes Γ_{slab} along the locus of the maximum of the 2D compressibility χ_{2D}. The direct observation of the critical fluctuations will be described in section 7.

6. Wetting near the bulk critical point

When the temperature increases toward the critical temperature T_c of the bulk fluid, the density–density correlation length ξ_{3D} becomes divergently large. Since ξ_{3D} gives the width of the interface between the liquid-like part and the gas-like part in the density profile of the wetting film, the slab model becomes less reliable on approaching T_c. In fact, although the slab model gives satisfactory results for d_{slab} and l_{slab} at 1386 °C, as shown in figure 14, our analysis reveals that the pressure variation of d_{slab} at 1440 °C exhibits a sudden downward inflection at a pressure (147.5 MPa) intermediate between the prewetting transition and the liquid–gas transition [44]. See figure 17(a), in which a similar pressure dependence of d_{slab} at 1484 °C is shown. Then, instead of the slab model, a hyperbolic tangent (hereafter abbreviated as tanh) model is adopted to include a smooth density profile, which is expressed as

$$d_l^{\tanh}(z) = \frac{1}{2}(d_l^{\tanh}(0) - d_{gas})[1 + \exp(-2l_{\tanh}/w_{\tanh})]\,[1 + \tanh(-(z - l_{\tanh})/w_{\tanh})] + d_{gas} \tag{11}$$

where $d_l^{\tanh}(0)$ is the density at $z = 0$, and $l_{\tanh}$ and $w_{\tanh}$ are parameters characterizing the thickness of the film and the broadness of the liquid–gas interface, respectively (see figure 6(b)).

The reflectivities R_p^{cal} and R_s^{cal} can be calculated for *any* permittivity profile $\epsilon(z)$ by solving Maxwell's equations numerically, where the following electromagnetic wave equations, (12) and (13), are transformed into first-order differential equations represented by 2×2 matrices [44]:

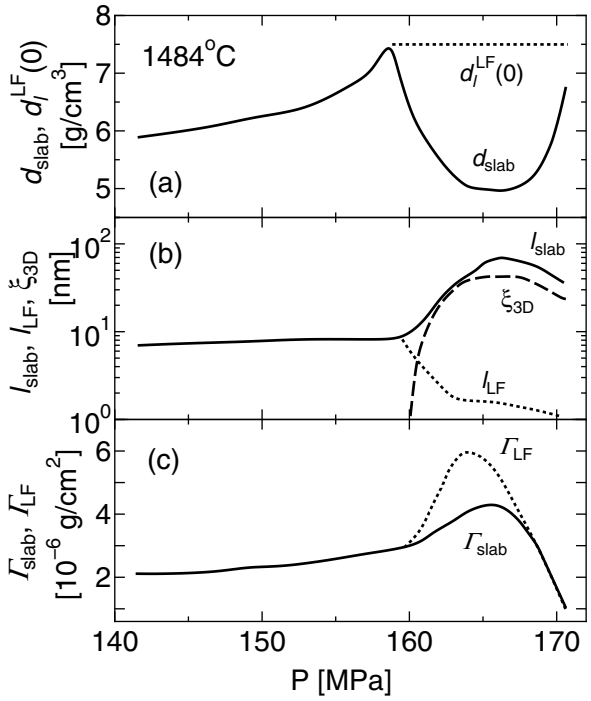

Figure 17. The solid lines indicate the density d_{slab} (a), the thickness l_{slab} (b) and the coverage Γ_{slab} (c) of the wetting film estimated from the reflectance data R_p and R_s at 1484 °C by using the slab model. The dotted line in (a), the dotted line in (b), the dashed line in (b) and the dotted line in (c) indicate the parameters estimated for the slowly varying power-law–exponential-type profile, $d_l^{LF}(0)$, l_{LF}, ξ_{3D} and Γ_{LF}, respectively (see equation (14)). In the present work, $d_l^{LF}(0)$ was fixed at 7.5 g cm^{-3}. The dashed line in (a) is the density of the bulk fluid mercury.

(i) For the s wave, the polarization vector is perpendicular to the plane of incidence, or, along the y-axis $\boldsymbol{e}_y$, and $\boldsymbol{E}(\boldsymbol{r})$ has the form $\boldsymbol{E}(\boldsymbol{r}) = E(z)\mathrm{e}^{\mathrm{i}k_x x}\boldsymbol{e}_y$. Then, $E(z)$ is calculated from the differential equation

$$\mathrm{d}^2E(z)/\mathrm{d}z^2 + q(z)^2E(z) = 0 \tag{12}$$

with

$$q(z)^2 = (2\pi/\lambda)^2(\tilde{\epsilon}(z) - n_0^2\sin^2\theta).$$

(ii) For the p wave, the magnetic field parallel to $\boldsymbol{e}_y$, $\boldsymbol{B}(\boldsymbol{r}) = B(z)\mathrm{e}^{\mathrm{i}k_x x}\boldsymbol{e}_y$, is calculated from

$$\frac{\mathrm{d}}{\mathrm{d}z}\left(\frac{1}{\tilde{\epsilon}(z)}\frac{\mathrm{d}B(z)}{\mathrm{d}z}\right) + \frac{q(z)^2}{\tilde{\epsilon}(z)}B(z) = 0. \tag{13}$$

Since only two independent data, R_p^{obs} and R_s^{obs}, are available to us, we have assumed the pressure dependence of $d_l^{tanh}(0)$ and optimized l_{tanh} and w_{tanh} by minimizing the discrepancy between the calculated and experimental reflectivities. In this procedure a reasonable density profile has been obtained at 1440 °C. We have also noticed that, although there are some ambiguities in determining the individual parameters, the coverage Γ, which is the order parameter, does not significantly depend on the choice of $d_l^{tanh}(0)$ or on the model adopted [44].

On further approaching the critical temperature, l_{tanh} in the tanh model has proved to become negative, implying that the density profile declines very steeply with increasing z.

Then, alternatively, we adopt a power-law–exponential-type adsorption profile which was proposed by Liu and Fisher [49] to explain the critical adsorption:

$$d_l^{\mathrm{LF}}(z) = P_0 t^{\beta_{3\mathrm{D}}} \left(\frac{1 + cz/\xi_{3\mathrm{D}}}{z/\xi_{3\mathrm{D}}} \right)^{\beta_{3\mathrm{D}}/\nu_{3\mathrm{D}}} \mathrm{e}^{-z/\xi_{3\mathrm{D}}} + d_{\mathrm{gas}}. \tag{14}$$

Here, t is the reduced temperature $t = (T - T_{\mathrm{c}})/T_{\mathrm{c}}$, and $\beta_{3\mathrm{D}}$ and $\nu_{3\mathrm{D}}$ are the critical exponents of bulk fluid. c is a constant and of the order of unity. The function $d_l^{\mathrm{LF}}(z) - d_{\mathrm{gas}}$ varies as $(z/\xi_{3\mathrm{D}})^{-\beta_{3\mathrm{D}}/\nu_{3\mathrm{D}}}$ for small $z/\xi_{3\mathrm{D}}$ and as $\mathrm{e}^{-z/\xi_{3\mathrm{D}}}$ for large $z/\xi_{3\mathrm{D}}$. This density profile satisfies the scaling law proposed by Fisher and de Gennes [50]. The critical exponents $\alpha_{3\mathrm{D}}$, $\beta_{3\mathrm{D}}$ and $\gamma_{3\mathrm{D}}$ of Hg have been estimated experimentally from the shape of the liquid–gas coexistence curve and the compressibility data [20,51]; the results reveal that they are all very close to the values expected from the 3D Ising model. Assuming the hyper-scaling law [52], which is valid when fluctuations are fundamentally important, we can also estimate $\nu_{3\mathrm{D}}$ from $\alpha_{3\mathrm{D}}$. The density profile is illustrated in figure 6(c), in which a cut-off density $d_l^{\mathrm{LF}}(0)$ for z smaller than a cut-off distance l_{LF} is introduced to suppress the divergence of the density in the small-z region. It should be noted that, when $\xi_{3\mathrm{D}} \ll l_{\mathrm{LF}}$, the density profile $d_l^{\mathrm{LF}}(z)$ coincides with that of the slab model $d_l^{\mathrm{slab}}(z)$ with $l_{\mathrm{slab}} = l_{\mathrm{LF}}$ and $d_{\mathrm{slab}} = d_l^{\mathrm{LF}}(0)$.

In figure 17 the densities (a), the various length scales (b) and the coverages (c) of the wetting film are shown at 1484 °C as functions of pressure [44]. The slab model results in a sudden decrease of d_{slab} and a sudden increase of l_{slab} at 160 MPa. In the Liu–Fisher model, $d_l^{\mathrm{LF}}(0)$ is fixed at 7.5 g cm^{-3}, which is close to the maximum of d_{slab}. It is reasonable that $\xi_{3\mathrm{D}}$ begins to rise sharply at 160 MPa and becomes very large in the bulk critical region. On the other hand, l_{LF} decreases drastically in the same pressure range. These facts suggest that the Liu–Fisher model is more appropriate than the slab model near the bulk critical point. The coverage Γ calculated from the parameters $d_l^{\mathrm{FL}}(0)$, l_{FL} and $\xi_{3\mathrm{D}}$ is larger than that calculated from the slab model, because the long-range tail of the density profile is included in the former calculation. Since these quantities are still fairly model dependent, we discuss only the qualitative aspects in what follows.

In figure 18 the state points where the sudden decrease of d_{slab} appears and those where l_{tanh} becomes zero are shown on the (P, T) plane together with the bulk coexistence curve, the locus of the maximum 3D compressibility $\chi_{3\mathrm{D}}$, the prewetting line and the locus of the maximum 2D compressibility $\chi_{2\mathrm{D}}$. The line of the sudden decrease of d_{slab} bends near the CPW. l_{tanh} becomes zero near the isochore for 4 g cm^{-3}, where $\chi_{3\mathrm{D}}$ begins to rise steeply, and it remains negative until the density of the background fluid becomes identical to $d_l^{\mathrm{tanh}}(0)$.

Hence, we believe that the rapid change in the density profile around 4 g cm^{-3} may be associated with the bulk critical phenomena. It may also be conceivable that the lateral fluctuations, which will be described in detail in the next section, cause the blurring of the density profile. However, since the optical emissivity does not change strongly at densities near to or above 4 g cm^{-3}, the lateral fluctuations should play a minor role in the present case. Thus one may consider the appreciable change in the density profile to be assignable to a crossover from the complete wetting to the critical adsorption [24]. This may imply that the bulk critical fluctuations could change the two-dimensional character of the interfacial phenomena into three-dimensional character.

7. Direct observation of the 2D critical fluctuations

The density profile $d_l(z)$ which we have discussed in the preceding sections is averaged over the lateral coordinates (x, y). However, in a real wetting film the number of adsorbed atoms should vary from place to place on the surface. In particular, the lateral fluctuations should be

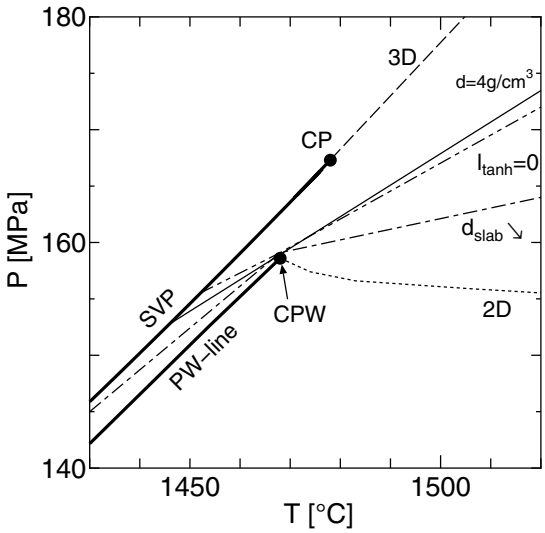

Figure 18. The dot–dashed line and the dot–dot–dashed line indicate the state points where the sudden decrease of $d_{\rm slab}$ appears and those where $l_{\rm tanh}$ becomes zero, respectively, on the (P, T) plane. $l_{\rm tanh}$ becomes zero near the isochore for 4 g cm^{-3}, denoted by the thin solid line. The bulk coexistence curve and the prewetting line are also indicated, by the thick solid lines. The dashed line and the dotted line indicate the loci of the maximum 3D and 2D compressibilities, respectively.

very large in the vicinity of the prewetting critical point. In order to describe such fluctuations, experimental information on the two-point correlation functions is required. Diffuse scattering experiments utilizing x-rays or neutrons constitute a powerful tool for studying the interfacial structure, and the theoretical basis is well established [53, 54]. However, the application of this technique to extreme conditions is very difficult at the present stage. Hence we need an alternative method. Recently, we have noticed that the thermal radiation emitted from the mercury–sapphire interface contains information not only on the reflectance but also on the diffuse scattering, and can be used to detect the lateral fluctuations in the wetting film [22].

In general, the thermal radiation emitted from a surface of some body can be related to its optical properties by using the following equation (Kirchhoff's law) [55]:

$$I_{\rm rad}(\omega, \theta) = A(\omega, \theta) \cos\theta I_{\rm BB}(\omega). \tag{15}$$

Here we denote the radiation intensity with frequency ω from a unit surface area at an angle θ to its normal by $I_{\rm rad}(\omega, \theta)$, and the black-body radiation intensity by $I_{\rm BB}(\omega)$. $A(\omega, \theta)$ is the 'absorbing power', and defined as the fraction of light absorbed by the body.

If the body is not transparent, the fraction of light which is *not* absorbed by the body, $1 - A(\omega, \theta)$, consists of a specular reflectivity term $R(\omega, \theta)$ and an off-specular diffuse scattering term due to the interfacial fluctuations. The scattering term should be integrated over the solid angle $\mathrm{d}\Omega' = \sin\theta' \, \mathrm{d}\theta' \, \mathrm{d}\varphi'$ into which the light is scattered. Thus $I_{\rm rad}$ can be written as

$$I_{\rm rad}(\omega, \theta) = I_{\rm BB}(\omega) \left[(1 - R(\omega, \theta)) \cos\theta - \int \mathrm{d}\Omega' \, \frac{1}{A} \frac{\mathrm{d}\sigma}{\mathrm{d}\Omega'} \right] \tag{16}$$

where $\mathrm{d}\sigma/\mathrm{d}\Omega'$ is the differential cross section of the diffuse scattering and A is an effective surface area of the interface.

Equation (16) may be understood from a Gedanken experiment similar to that carried out by Kirchhoff about 150 years ago [56]. Consider the body in thermal equilibrium with

the black-body radiation surrounding it, as shown schematically in figure 19. Because of the thermal equilibrium, the black-body radiation falling onto unit surface area of the body at an angle θ, $\cos\theta\, I_{\mathrm{BB}}(\omega)$, should be balanced by that leaving the surface of the body. The latter radiation consists of the emission from the body, $I_{\mathrm{rad}}(\omega, \theta)$, and the reflection or scattering of the black-body radiation from other directions:

$$I_{\mathrm{BB}}(\omega)\left[R(\omega,\theta)\cos\theta + \int \mathrm{d}\Omega' \,\frac{1}{A}\frac{\mathrm{d}\sigma}{\mathrm{d}\Omega'}\right].$$

By equating the intensities of these two radiations, we can obtain equation (16).

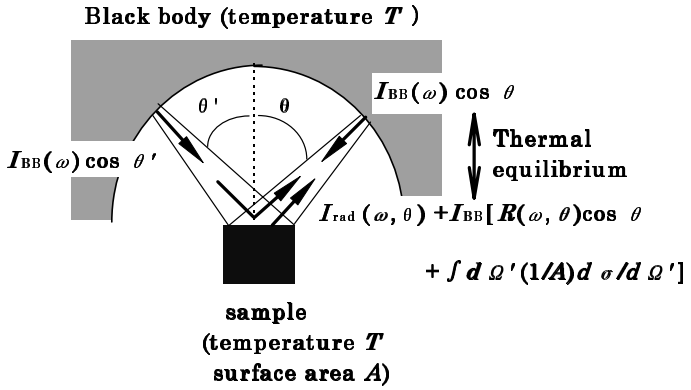

Figure 19. A gedanken experiment for deriving the intensity of the thermal radiation, $I_{\mathrm{rad}}(\omega, \theta)$, from some body with temperature T. (See equations (15) and (16).) The body is in thermal equilibrium with the black-body radiation surrounding it.

In the present case, 'the body' means the mercury sample behind the sapphire rod, and the surrounding molybdenum cavity. The area bounded by the dashed line in figure 20 indicates 'the body' conceptually. The reflectivity and the scattering cross section in equation (16) are considered to be those at the mercury–sapphire interface. Note that only surface terms appear in equation (16), because all of the light that penetrates deep into the cavity beyond the interface is expected to be absorbed by the bulk fluid mercury or the molybdenum cavity wall, which can be considered as a black body.

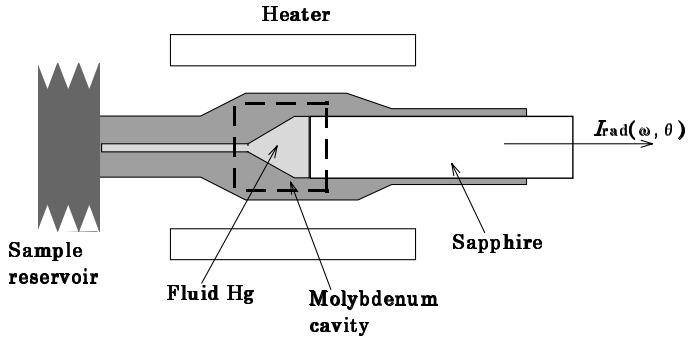

Figure 20. A schematic illustration of the sample cell for measuring the thermal radiation intensity. The area bounded by the dashed line indicates 'the body', which emits the thermal radiation $I_{\mathrm{rad}}(\omega, \theta)$.

We have made simultaneous measurements of the optical reflectivity R_n at 1064 nm and the thermal radiation I_{rad} at 1550 nm [22]. Figure 21(a) shows the results for R_n and I_{rad} at a subcritical temperature. The radiation intensity shows a remarkable change both at the prewetting transition and at the liquid–gas transition. It should be noticed that the changes of I_{rad} are nearly opposite to those of R_n. A more interesting observation has been made at the supercritical temperatures (see figure 21(b)), where the radiation intensity exhibits a deep minimum although the reflectivity varies more gently. In this case the second term on the right-hand side in equation (16), corresponding to the diffuse scattering due to the permittivity fluctuations at the interface between the Hg wetting film and Hg vapour, should play a major role. It has been proved that the permittivity fluctuations become the largest on the locus of the χ_{2D}-maximum (the dashed line in figure 3) [22].

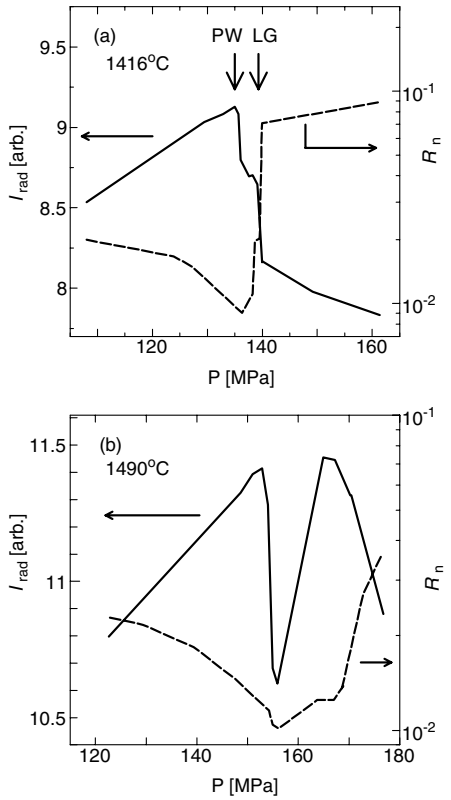

Figure 21. The thermal radiation intensity at 1550 nm (solid line) and the reflectivity at 1064 nm (dashed line) measured at constant temperatures of 1416 °C ($<T_{pw}^{c}$) (a) and 1490 °C ($>T_{pw}^{c}$) (b) [22]. In (a), the prewetting and liquid–gas transitions are indicated by 'PW' and 'LG', respectively.

The permittivity fluctuations at the interface between the Hg wetting film and Hg vapour may be estimated from the diffuse scattering contribution to the thermal radiation intensity. Within the framework of the modified first Born approximation, the scattering cross section can be expressed in terms of the Fourier transform, $G(\vec{p}, z, z')$, of the two-point correlation function, $\langle\tilde{\epsilon}^*(\vec{r}, z)\tilde{\epsilon}(\vec{r'}, z')\rangle$, of the permittivity fluctuation $\tilde{\epsilon}(\vec{r}, z)$ [54]:

$$\frac{1}{A}\frac{d\sigma}{d\Omega'} \propto \frac{1}{\lambda^4}\int dz \int dz'\, G(\vec{p}, z, z')F(z, z'). \tag{17}$$

Here, $\vec{r} = (x, y)$ is the lateral direction, $\vec{p}$ is the momentum transfer parallel to the surface and

$$|\vec{p}|^2 = (2\pi n_0/\lambda)^2(\sin^2\theta + \sin^2\theta' + 2\sin\theta\sin\theta'\cos\varphi').$$

z is the coordinate normal to the surface, and $z = 0$ at the sapphire substrate. $F(z, z')$ is related to the electric fields at z and z', and is a slowly varying function of z and z'. $F(z, z')$ also depends on the incident and the scattering directions. We made the assumption that $G(\vec{p}, z, z')$ has a functional form of the Ornstein–Zernike type:

$$G(\vec{p}, z, z') \propto \begin{cases} \xi_{2D}^2 |\Delta\epsilon|^2 / (1 + \xi_{2D}^2 p^2) & \text{for } l - \Delta l/2 < z, z' < l + \Delta l/2 \\ 0 & \text{otherwise} \end{cases} \tag{18}$$

where ξ_{2D} is the correlation length in the lateral plane, l is mean thickness of the wetting film, Δl is the thickness of the fluctuating region of the film/vapour interface and $\Delta\epsilon$ is the strength of the permittivity fluctuation.

As a first approximation, we have assumed that the correlation length ξ_{2D} is much smaller than the wavelength of the light, $\lambda = 1550$ nm. In this case, $G(\vec{p}, z, z')$ is nearly equal to $G(0, z, z')$, and the integration of the scattering cross section over the solid angle Ω' in equation (16) becomes considerably simplified. Figure 22 shows the estimated quantity $(\Delta l)^2\xi_{2D}^2 |\Delta\epsilon|^2$, which is a measure of the interfacial fluctuation. When the temperature is lower than that of the CPW, the quantity $(\Delta l)^2\xi_{2D}^2 |\Delta\epsilon|^2$ jumps at the prewetting transition, and then diverges when the liquid–gas transition is approached. In the prewetting supercritical region, $(\Delta l)^2\xi_{2D}^2 |\Delta\epsilon|^2$ exhibits a peak, which corresponds to the maximum of $\chi_{2D} = (\partial\Gamma/\partial\mu)_T$. The peak becomes broader with increasing temperature.

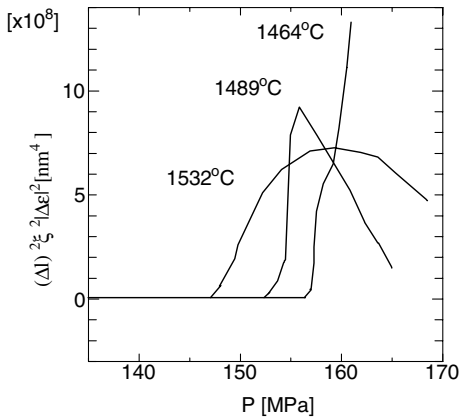

Figure 22. Estimated values of $(\Delta l)^2\xi^2 |\Delta\epsilon|^2$, which is a measure of the interfacial fluctuation [22].

The above measurements were done for radiation with the single wavelength $\lambda = 1550$ nm. We are now trying to measure the wavelength dependence of the radiation intensity by using a spectrometer, and to determine the p-dependence of $G(p, z, z')$ and the correlation length ξ_{2D} unambiguously (see equation (18)). Because p is of the order of $2\pi/\lambda$, the denominator in equation (18) deviates from unity when λ is comparable to or smaller than ξ_{2D}. Figure 23 shows a preliminary result for the scattering intensity multiplied by λ^4 at 1500 °C in the wavelength range from 500 to 1000 nm. The factor λ^4 is needed to eliminate the Rayleigh 'blue-sky factor'. The scattering cross section increases with decreasing $2\pi/\lambda$ as is expected from equation (18). In particular, around the maximum of the 2D compressibility (∼156 MPa), the slope of the curve is remarkably large, indicating that ξ_{2D} becomes very large and comparable

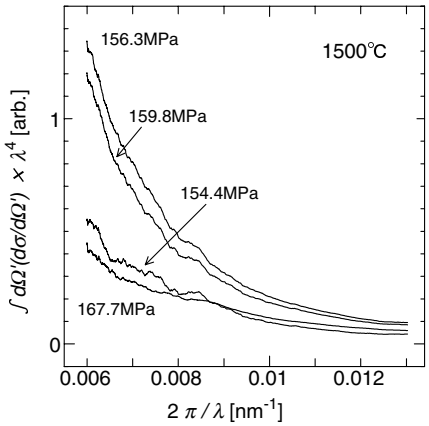

Figure 23. The scattering cross section $\int \mathrm{d}\Omega' \, (\mathrm{d}\sigma/\mathrm{d}\Omega')$ multiplied by λ^4 to eliminate the Rayleigh 'blue-sky factor', measured at 1500 °C as a function of the wavenumber $2\pi/\lambda$ [57].

to the wavelength of light λ in this region. From curve fitting, the peak of the correlation length ξ_{2D} is estimated to be of the order of several hundred nanometres. Further details will be given elsewhere [57].

Recently, Omata and Yonezawa [58] have carried out Monte Carlo simulations and a simple density functional calculation for Lennard-Jones systems. They have investigated the prewetting supercritical phase, and shown that density fluctuations in a wetting film play an important role. From structure factors of the first adsorption layer, they derived isotherms of 2D compressibility and a correlation length. They have shown that the locus of the maximum 2D compressibility appears at considerably lower pressures than the simple extrapolation of the prewetting line, and this coincides with the present results of mercury-on-sapphire experiments, as shown by the dashed lines in figure 3 and figure 8.

8. Summary

In the present article we have described the present status of the studies on the wetting phenomena for mercury on sapphire. The major results are as follows:

(1) We have found a prewetting transition at the Hg/sapphire interface and determined the wetting phase diagram. The wetting temperature is about 1310 °C, and the prewetting critical temperature and pressure are 1468 °C and 158.6 MPa, respectively.
(2) We have developed an ellipsometric method that can be applied to high-temperature fluids contacting a sapphire window, and this enables us to determine the coverage of the Hg film. On the basis of the estimated density of the wetting film, we have suggested that the Hg film should be non-metallic.
(3) We have suggested the possibility of a crossover from complete wetting to critical adsorption in the vicinity of the bulk critical point.
(4) We have found that the thermal radiation can be utilized to probe the interfacial fluctuations. A sharp dip in the thermal radiation intensity is observed in the region where the 2D compressibility becomes maximum.

To promote better understanding of the interfacial phenomena of the Hg/sapphire system, not only the accumulation of more accurate experimental data but also theoretical works in which the electronic properties are properly taken into account are required.

Acknowledgments

We would like to express sincere thanks to Professor F Hensel, who led us to the field of wetting phenomena. We also thank Mr Y Kajihara for collaboration. We are also very grateful to Professors S Dietrich and Dr K Omata for valuable discussions.

References

[1] Dietrich S 1988 *Phase Transitions and Critical Phenomena* ed C Domb and J L Lebowitz (New York: Academic) p 1
[2] Cahn J W 1977 *J. Chem. Phys.* **66** 3667
[3] Hauge E H and Schick M 1983 *Phys. Rev.* B **27** 4288
[4] Nicolaides D and Evans R 1989 *Phys. Rev.* B **39** 9336
Nicolaides D and Evans R 1989 *Phys. Rev. Lett.* **63** 778
[5] Kellay H, Bonn D and Meunier J 1993 *Phys. Rev. Lett.* **71** 2607
[6] Lucht R and Bahr Ch 1998 *Phys. Rev. Lett.* **80** 3783
[7] Ebner C and Saam W F 1977 *Phys. Rev. Lett.* **38** 1486
[8] Ebner C and Saam W F 1987 *Phys. Rev.* B **35** 1822
[9] Rutledge J E and Taborek P 1992 *Phys. Rev. Lett.* **69** 937
[10] Cheng E, Cole M W, Dupont-Roc J, Saam W F and Treiner J 1993 *Rev. Mod. Phys.* **65** 557
[11] Cheng E, Mistura G, Lee H C, Chan M H W, Cole M W, Carraro C, Saam W F and Toigo F 1993 *Phys. Rev. Lett.* **70** 1854
[12] Yao M and Hensel F 1996 *J. Phys.: Condens. Matter* **8** 9547
[13] Kozhevnikov V F, Arnold D I, Naurzakov S P and Fisher M E 1997 *Phys. Rev. Lett.* **78** 1735
[14] Wyatt A F G, Klier J and Stefanyi P 1995 *Phys. Rev. Lett.* **74** 1151
Phillips J A, Ross D, Taborek P and Rutledge J E 1998 *Phys. Rev.* B **58** 3361
[15] Tostmann H, Nattland D and Freyland W 1996 *J. Chem. Phys.* **104** 8777
[16] Hensel F and Yao M 1995 *Elementary Processes in Dense Plasmas* ed S Ichimaru and S Ogata (Reading, MA: Addison-Wesley) p 295
Hensel F 1995 *Adv. Phys.* **44** 3
Hensel F and Yao M 1996 *J. Non-Cryst. Solids* **205–207** 231
[17] Dzyaloshinskii I E, Lifshitz E M and Pitaevskii L P 1961 *Adv. Phys.* **10** 165
[18] Israelachvili J N 1992 *Intermolecular and Surface Forces* 2nd edn (New York: Academic) ch 11
[19] Ashcroft N W and Stroud D 1978 *Solid State Physics* vol 33 (New York: Academic) p 2
[20] Hensel F and Warren W W Jr 1999 *Fluid Metals* (Princeton, NJ: Princeton University Press) ch 4
[21] See e.g. Logan D E and Edwards P P 1986 *Phil. Mag.* B **53** L23
[22] Ohmasa Y, Kajihara Y, Kohno H, Hiejima Y and Yao M 2000 *J. Phys.: Condens. Matter* **12** A375
[23] Heidel B and Findenegg G H 1987 *J. Chem. Phys.* **87** 706 and references therein
[24] Dietrich S 1991 *Phase Transitions in Surface Films 2* ed H Taub *et al* (New York: Plenum)
[25] Warren Jr W W and Hensel F 1982 *Phys. Rev.* B **26** 966
[26] Yao M, Hayami W and Endo H 1990 *J. Non-Cryst. Solids* **117/118** 473
Yao M 1994 *Z. Phys. Chem.* **184** 73
[27] Car R and Parrinello M 1985 *Phys. Rev. Lett.* **55** 2471
[28] Kresse G and Hafner J 1997 *Phys. Rev.* B **55** 7539
[29] Yao M and Endo H 1982 *J. Phys. Soc. Japan* **51** 966
[30] Suzuki K, Inutake M, Fujiwaka S, Yao M and Endo H 1980 *J. Physique Coll.* **41** C8 66
[31] Tamura K, Inui M, Nakaso I, Oh'ishi Y, Funakoshi K and Utsumi W 1999 *J. Non-Cryst. Solids* **250/252** 148
[32] Einstein A and Gingrich N S 1942 *Phys. Rev.* **62** 261
[33] Franz G, Freyland W, Gläser W, Hensel F and Schneider E 1980 *J. Physique Coll.* **41** C8 194
[34] Winter R, Bodensteiner T, Gläser W and Hensel F 1987 *Ber. Bunsenges. Phys. Chem.* **91** 1327
[35] Tamura K and Hosokawa S 1998 *Phys. Rev.* B **58** 9030
[36] Kohno H and Yao M 1999 *J. Phys.: Condens. Matter* **11** 5399
[37] Born M and Wolf E 1980 *Principles of Optics* 6th edn (New York: Pergamon) ch 1
[38] Berning H P 1963 *Physical Properties of Thin Films* vol 1, ed G Hass (New York: Academic)
[39] Hensel F and Yao M 1997 *Eur. J. Solid State Inorg. Chem.* **34** 861
Hensel F and Yao M 1998 *Ber. Bunsenges. Phys. Chem.* **102** 1798

[40] Azzam R M A and Bashara N M 1987 *Ellipsometry and Polarized Light* paperback edn (Amsterdam: North-Holland) ch 4
[41] Nattland D and Freyland W 1988 *Phys. Rev. Lett.* **60** 1142
[42] Ohmasa Y, Kajihara Y and Yao M 1998 *J. Phys.: Condens. Matter* **10** 11 589
[43] Ohmasa Y, Kajihara Y, Kohno H, Hiejima Y and Yao M 1999 *J. Non-Cryst. Solids* **250–252** 209
[44] Ohmasa Y, Kajihara Y and Yao M 2001 *Phys. Rev.* E **63** at press
[45] Taborek P and Rutledge J E 1993 *Phys. Rev. Lett.* **71** 263
[46] Staroske S, Nattland D and Freyland W 2000 *Phys. Rev. Lett.* **84** 1736
[47] Hensel F and Warren W W Jr 1999 *Fluid Metals* (Princeton, NJ: Princeton University Press) ch 6.4
[48] Hefner W 1980 *Doctoral Thesis* Marburg University
[49] Liu A J and Fisher M E 1989 *Phys. Rev.* A **40** 7202 and references therein
[50] Fisher M E and de Gennes P-G 1978 *C. R. Acad. Sci.* B **287** 207
[51] Götzlaff W 1988 *Doctoral Thesis* Marburg University
[52] Privman V, Hohenberg P C and Aharony A 1989 *Phase Transitions and Critical Phenomena* vol 14, ed C Domb and J L Lebowitz (New York: Academic)
[53] Sinha S K, Sirota E B, Garoff S and Stanley H B 1988 *Phys. Rev.* B **38** 2297
[54] Dietrich S and Haase A 1995 *Phys. Rep.* **260** 1
[55] Planck M 1914 *The Theory of Heat Radiation* part I (Philadelphia: Blakiston) ch 2
Landau L D and Lifshitz E M 1958 *Statistical Physics* (New York: Pergamon) ch 5, section 60
[56] Kirchhoff G R 1859 *Monatsber. Akad. Wiss. Berlin* (December)
Kirchhoff G R 1860 *Poggendorff Ann.* **109** 275
[57] Kajihara Y, Ohmasa Y and Yao M 2001 to be published
[58] Omata K and Yonezawa F 1998 *J. Phys.: Condens. Matter* **10** 9431
Omata K and Yonezawa F 1999 *J. Non-Cryst. Solids* **250–252** 214
Omata K and Yonezawa F 2000 *Prog. Theor. Phys. Suppl.* **138** 268